Progress In Electromagnetics Research C, Vol. 84, 147–160, 2018

The Properties of the Electromagnetic Scattering from a Sinusoidal Water Wave

Yunhua Wang[1, 2], Yue Yu[1], Yanmin Zhang[1, *], and Honglei Zheng[1]

Abstract—Within the framework of the higher-order Kirchhoff approximation, the properties of the electromagnetic scattering from sinusoidal water waves are presented, and the theoretical formulas up to third-order for describing the scattering field and its spectrum are derived. It shows that not only the spectral peaks which correspond to phase velocity of the water wave but also other discrete harmonic peaks can be found from the theoretical spectrum model. And the Doppler shifts of the spectral peaks are all integral multiple of the sinusoidal wave's frequency. For the backscattering field from a sinusoidal wave, the higher-order resonant peaks would also be found at different scattering angles, and the values of these peaks decrease with the scattering angle. On the other hand, the comparisons with the MoM demonstrate that the contributions of the slope-dependent terms can be generally neglected if the amplitude of the sinusoidal wave is small. However, if the waves slope is larger, the impact of the second order scattering becomes obvious and cannot be omitted.

1. INTRODUCTION

The study on electromagnetic scattering from rough surface has been the subject of intensive investigation over the past decades for its application in land and ocean remote sensing [1–14]. Normalized radar cross section (NRCS), frequency spectrum and polarimetric properties are generally used to describe scattering fields. Among these parameters, NRCS and frequency spectrum reflect the intensity of the scattering field and the line-of-sight velocity of the scatterers, respectively. In the area of ocean remote sensing, NRCS and Doppler behaviors of sea echoes have been widely used to retrieve wind field [5], sea wave spectrum [6–10] and sea surface current [11–14]. It is well known that the actual sea surface can be represented by a sum of sine waves based on the linear theory [15]. Thus, it is necessary to investigate the scattering field from a sinusoidal water wave in order to understand the properties of electromagnetic scattering from sea surface. Up to now, many analytic and numerical methods, such as Kirchhoff approximation (KA), small perturbation method (SPM), and method of moment (MoM), have been developed to evaluate NRCS and Doppler spectrum [1–4, 16–25] of the electromagnetic scattering from an oceanic surface. Although MoM is an exact numerical method to calculate electromagnetic scattering from rough surface, and the Doppler spectra of the scattering fields from water surfaces can be well simulated by it, the theoretical spectral model cannot be derived directly by MoM. Among analytic methods, KA has been widely used as the method for describing scattering from sea surface, and higher-order KA can be used to analyze the influence of the surface slope on the scattering fields [26] conveniently. Thus, in the present work, the scattering fields from a sinusoidal water wave are simulated using higher-order KA, and the influences of slope-dependent higher order scattering terms are also discussed.

Received 20 March 2018, Accepted 17 May 2018, Scheduled 31 May 2018
* Corresponding author: Yanmin Zhang (yanminzhang@ouc.edu.cn).
[1] College of Information Science & Engineering, Ocean University of China, China. [2] Laboratory for Regional Oceanography and Numerical Modeling, Qingdao National Laboratory for Marine Science and Technology, China.

In Section 2, the theoretical formulas up to third-order for the NRCS and Doppler spectrum are derived within the framework of the higher-order Kirchhoff approximation. And the interesting phenomenon can be well explained by the formulas proposed by us. Section 3 is devoted to the results and the discussions while the concluding remarks and perspectives are provided in Section 4.

2. THE SCATTERING FIELD AND THE DOPPLER SPECTRUM

If the RMS slope of a water surface is less than 0.25, a scalar approximation of the Kirchhoff method can be used to evaluate the scattering field of the water surface. And the expression of the scattering field can be written as [26]

$$E_{pq}^{s} = K \int \bar{U}_{pq} \exp\left[jk_e\left(\hat{\mathbf{k}}_s - \hat{\mathbf{k}}_i\right)\cdot\mathbf{r}\right] \mathrm{d}\mathbf{r} \tag{1}$$

where $K = \frac{ik_e}{4\pi R}\exp(jk_eR)$, k_e is the wavenumber of the incident electromagnetic wave, and R denotes the range from surface center to radar. The subscripts 'p' and 'q' denote 'h' or 'v'. The unit vector wavenumbers $\hat{\mathbf{k}}_i$ and $\hat{\mathbf{k}}_s$ can be expressed as $\hat{\mathbf{k}}_i = (\hat{\mathbf{x}}\sin\theta_i\cos\phi_i + \hat{\mathbf{y}}\sin\theta_i\sin\phi_i - \hat{\mathbf{z}}\cos\theta_i)$ and $\hat{\mathbf{k}}_s = \hat{\mathbf{x}}\sin\theta_s\cos\phi_s + \hat{\mathbf{y}}\sin\theta_s\sin\phi_s + \hat{\mathbf{z}}\cos\theta_s$. θ_i and θ_s denote the incident and the scattering angles, and ϕ_i and ϕ_s denote the azimuth angles, respectively.

Based on the periodogram methods, the Doppler spectrum of the scattered field can be expressed as

$$\begin{aligned} S(\omega) &= \left\langle E_{pq}^{s}(\omega)\cdot E_{pq}^{s*}(\omega)\right\rangle \\ &= |K|^2 \iiint \left\langle \bar{U}_{pq}\bar{U}_{pq}^{*}\exp\left[jk_e\left(\hat{\mathbf{k}}_s - \hat{\mathbf{k}}_i\right)\cdot\left(\mathbf{r}-\mathbf{r}'\right)\right]\right\rangle \exp\left(j\omega t - j\omega t'\right)\mathrm{d}\mathbf{r}\mathrm{d}\mathbf{r}'\mathrm{d}t\mathrm{d}t' \end{aligned} \tag{2}$$

where $E_{pq}^{s}(\omega) = K\int\int \bar{U}_{pq}\Psi\exp(j\omega t)\mathrm{d}\mathbf{r}\mathrm{d}t$ is the Fourier transform of the scattered field. T denotes the time length of the series $E_{pq}^{s}(t)$. For different polarizations, the factor $\bar{U}_{pq}$ is of the form $\bar{U}_{pq} = a_0 + a_1Z_x + a_2Z_y$, then we can write the product $\bar{U}_{pq}\bar{U}_{pq}^{*}$ up to second order in slope as

$$\begin{aligned} \bar{U}_{pq}\bar{U}_{pq}^{*} &= a_0a_0^{*} + a_0a_1^{*}Z_x' + a_0a_2^{*}Z_y' + a_1a_0^{*}Z_x + a_2a_0^{*}Z_y \\ &\quad + a_1a_1^{*}Z_xZ_x' + a_1a_2^{*}Z_xZ_y' + a_2a_1^{*}Z_yZ_x' + a_2a_2^{*}Z_yZ_y' \end{aligned} \tag{3}$$

here, a_0, a_1 and a_2 are all polarization-dependent coefficients [26].

2.1. The First-Order Spectrum

In Eq. (2), if we set $\bar{U}_{pq}\bar{U}_{pq}^{*} \approx a_0a_0^{*}$, then the first-order spectrum of the scattering field is obtained as

$$\begin{aligned} S_1(\omega) &= 4\pi R^2\frac{|Ka_0|^2}{T^2L^2}\int_{-T}^{T}\int_{-L}^{L}\int_{-L}^{L}(L-|u|)(L-|v|)(T-|\tau|) \\ &\quad \exp\left\{jq_xu + jq_yv - q_z^2\delta^2(1-\rho)\right\}\exp(j\omega\tau)\mathrm{d}u\mathrm{d}v\mathrm{d}\tau \end{aligned} \tag{4}$$

where $u = x_0 - x_0'$, $v = y_0 - y_0'$ and $\tau = t - t'$. δ^2 and ρ denote the variance and the correlation coefficient of the water wave.

For a monochromatic water wave, its profile can be expressed as

$$Z(x,y,t) = a\cos(k_{wx}x + k_{wy}y + \omega_w t) \tag{5}$$

where k_{wx} and k_{wy} denote the spatial wavenumber along $\hat{x}$ and $\hat{y}$ directions, respectively. $\omega_w = \sqrt{gk_w}$ with $k_w = (k_{wx}^2 + k_{wy}^2)^{1/2}$. Using Eq. (5), variance δ^2 and correlation coefficient ρ for the water wave can be obtained as

$$\delta^2 = \left\langle Z^2(x,y,t)\right\rangle = \frac{a^2}{2} \tag{6}$$

$$\rho(u,v,\tau) = \frac{\langle Z(x+u,y+v,t+\tau)Z(x,y,t)\rangle}{\langle Z^2(x,y,t)\rangle} = \cos[k_{wx}u + k_{wy}v + \omega_w\tau] \tag{7}$$

Suppose that the amplitude of the water wave is small, i.e., $q_z^2\delta^2 \ll 1$, and then the exponential term $\exp\{q_z^2\delta^2\rho\}$ in Eq. (4) can be expressed as a Taylor series, i.e.,

$$\exp\left(q_z^2\delta^2\rho\right) = \sum_{n=0}^{\infty} \frac{\left(q_z^2\delta^2\rho\right)^n}{n!} \tag{8}$$

Substituting Eqs. (6)–(8) into Eq. (4), the first-order spectrum $S_1(\omega)$ is rewritten as

$$\begin{aligned} S_1(\omega) \;=\; & 4\pi R^2 \frac{|Ka_0|^2}{T^2L^2} \exp\left\{-\frac{a^2q_z^2}{2}\right\} \cdot \sum_{n=0}^{\infty} \frac{\left\{q_z^2a^2\right\}^n}{2^n n!} \\ & \int_{-T}^{T}\int_{-L}^{L}\int_{-L}^{L} \cos^n[k_{wx}u + k_{wy}v - \omega_w\tau](L-|u|)(L-|v|)(T-|\tau|) \\ & \exp[jq_xu + jq_yv]\exp(j\omega\tau)\mathrm{d}u\mathrm{d}v\mathrm{d}\tau \end{aligned} \tag{9}$$

Using Euler's Formula, the power of cosine function can be rewritten as

$$\cos^n(k_{wx}u + k_{wy}v + \omega_w\tau) = \frac{1}{2^n}\sum_{r=0}^{n} C_n^r \exp[j(n-2r)(k_{wx}u + k_{wy}v + \omega_w\tau)] \tag{10}$$

where $C_n^r = \frac{n!}{r!(n-r)!}$ is the binomial coefficient. Substituting Eq. (10) into Eq. (9), after a tedious but straightforward derivation, the expression of the first-order spectrum is obtained as

$$\begin{aligned} S_1(\omega) \;=\; & 4\pi R^2|Ka_0|^2 \exp\left(-\frac{q_z^2a^2}{2}\right) \sum_{n=0}^{\infty}\sum_{r=0}^{\infty} \frac{\left(q_z^2a^2\right)^{2r+n}}{2^{4r+2n}} \frac{1}{r!(r+n)!} \\ & \left\{ Sa^2\left(\frac{q_x \pm nk_{wx}}{2}L\right) Sa^2\left(\frac{q_y \pm nk_{wy}}{2}L\right) Sa^2\left(\frac{\omega \pm n\omega_w}{2}T\right)\right\} \end{aligned} \tag{11}$$

where $Sa(X) = \sin(X)/X$ is the sampling function.

2.2. The Second- and the Third-Order Spectra

The other contribution to the total spectrum comes from the slope terms in Eq. (3). The second- and third-order spectra are written as

$$\begin{aligned} S_2(\omega) \;=\; & \frac{4\pi R^2\left|K\right|^2}{T^2L^2} \iint \left\langle \left(a_0a_1^*Z_x' + a_0^*a_1Z_x + a_0a_2^*Z_y' + a_2a_0^*Z_y\right) \exp\left[jk_e\left(\hat{\mathbf{k}}_s - \hat{\mathbf{k}}_i\right)\cdot\left(\mathbf{r}-\mathbf{r}'\right)\right]\right\rangle \\ & \cdot \exp\left(j\omega t - j\omega t'\right)\mathrm{d}\mathbf{r}\mathrm{d}\mathbf{r}'\mathrm{d}t\mathrm{d}t' \end{aligned} \tag{12}$$

and

$$\begin{aligned} S_3(\omega) \;=\; & \frac{4\pi R^2\left|K\right|^2}{T^2L^2} \iint \left\langle \left(a_1a_1^*Z_xZ_x' + a_1a_2^*Z_xZ_y' + a_2a_1^*Z_yZ_x' + a_2a_2^*Z_yZ_y'\right)\right. \\ & \left.\cdot \exp\left[jk_e\left(\hat{\mathbf{k}}_s - \hat{\mathbf{k}}_i\right)\cdot\left(\mathbf{r}-\mathbf{r}'\right)\right]\right\rangle \exp\left(j\omega t - j\omega t'\right)\mathrm{d}\mathbf{r}\mathrm{d}\mathbf{r}'\mathrm{d}t\mathrm{d}t' \end{aligned} \tag{13}$$

Using the following equations, i.e.,

$$\left\langle \exp(ja_1X_1 + ja_2X_2)X_3\right\rangle \;=\; -j\left.\frac{\partial\left\langle\exp(ja_1X_1 + ja_2X_2 + ja_3X_3)\right\rangle}{\partial a_3}\right|_{a_3=0} \tag{14}$$

$$\left\langle \exp\left(ja_1X_1 + ja_2X_2\right)X_3X_4\right\rangle \;=\; -\left.\frac{\partial^2\left\langle\exp(ja_1X_1 + ja_2X_2 + ja_3X_3 + ja_4X_4)\right\rangle}{\partial a_3\partial a_4}\right|_{a_3=a_4=0} \tag{15}$$

and

$$\left\langle \exp(ja_1X_1 + ja_2X_2 + \ldots + ja_NX_N)\right\rangle = \exp\left\{-\frac{1}{2}\sum_{m=1}^{N}\sum_{n=1}^{N} a_ma_n\left\langle X_mX_n\right\rangle\right\}, \tag{16}$$

the second- and third-order spectra can be rewritten as

$$S_2(\omega) = -j\frac{4\pi R^2 |K|^2 q_z a^2}{T^2 L^2}\int_{-T}^{T}\int_{-L}^{L}\int_{-L}^{L}(L-|u|)(L-|v|)(T-|\tau|)\left[\mathrm{Re}(a_0 a_1^*)\frac{\partial\rho}{\partial u}+\mathrm{Re}(a_0 a_2^*)\frac{\partial\rho}{\partial v}\right] \exp\left[jq_x u + jq_y v - q_z^2\delta^2(1-\rho)\right]\exp(j\omega\tau)\mathrm{d}u\mathrm{d}v\mathrm{d}\tau \quad (17)$$

and

$$S_3(\omega) = \frac{4\pi R^2 |K|^2}{T^2 L^2}\int_{-T}^{T}\int_{-L}^{L}\int_{-L}^{L}(L-|u|)(L-|v|)(T-|\tau|) \left\{\frac{a^2\rho}{2}\left[a_1 a_1^* k_{wx}^2 + a_2 a_2^* k_{wy}^2 + 2\mathrm{Re}(a_1 a_2^*)k_{wx}k_{wy}\right] -\frac{q_z^2 a^4}{4}\left[a_1 a_1^*\left(\frac{\partial\rho}{\partial u}\right)^2 + a_2 a_2^*\left(\frac{\partial\rho}{\partial v}\right)^2 + 2\mathrm{Re}\left(a_1 a_2^*\right)\left(\frac{\partial\rho}{\partial u}\right)\left(\frac{\partial\rho}{\partial v}\right)\right]\right\} \cdot\exp\left[jq_x u + jq_y v - q_z^2\delta^2(1-\rho)\right]\exp(j\omega\tau)\mathrm{d}u\mathrm{d}v\mathrm{d}\tau \quad (18)$$

with

$$\frac{\partial\rho}{\partial u} = -k_{wx}\sin(k_{wx}u + k_{wy}v + \omega_w\tau) \quad (19)$$

$$\frac{\partial\rho}{\partial v} = -k_{wy}\sin(k_{wx}u + k_{wy}v + \omega_w\tau) \quad (20)$$

Using Euler's Formula and substituting Eqs. (10), (19) and (20) into Eqs. (17)–(18), after a tedious but straightforward derivation, the expression of the second- and third-order spectra are both obtained as

$$S_2(\omega) = 2\pi R^2 |K|^2 a^2 q_z \exp\left(-\frac{q_z^2 a^2}{2}\right)\left\{\mathrm{Re}\left(a_0 a_1^*\right)k_{wx} + \mathrm{Re}\left(a_0 a_2^*\right)k_{wy}\right\}\sum_{n=0}^{\infty}\sum_{r=0}^{\infty}\frac{\left(q_z^2 a^2\right)^{2r+n}}{2^{4r+2n}}\frac{1}{r!(r+n)!} \left\{Sa^2\left(\frac{q_x+(n\pm1)k_{wx}}{2}L\right)Sa^2\left(\frac{q_y+(n\pm1)k_{wy}}{2}L\right)Sa^2\left(\frac{\omega+(n\pm1)\omega_w}{2}T\right) -Sa^2\left(\frac{q_x-(n\pm1)k_{wx}}{2}L\right)Sa^2\left(\frac{q_y-(n\pm1)k_{wy}}{2}L\right)Sa^2\left(\frac{\omega-(n\pm1)\omega_w}{2}T\right)\right\} \quad (21)$$

and

$$S_3(\omega) = \pi R^2 |K|^2 a^4 q_z^2 (k_{wx}^2 a_1 a_1^* + 2k_{wx}k_{wy}\mathrm{Re}\left(a_1 a_2^*\right) + k_{wy}^2 a_2 a_2^*)\exp\left(-\frac{q_z^2 a^2}{2}\right) \cdot\sum_{n=0}^{\infty}\sum_{r=0}^{\infty}\frac{\left(q_z^2 a^2\right)^{2r+n}}{2^{4r+2n}}\frac{1}{r!(r+n)!}\left\{S_{31}(\omega)+S_{32}(\omega)+S_{33}(\omega)\right\} \quad (22)$$

with

$$S_{31}(\omega) = \left\{Sa^2\left(\frac{q_x+(n\pm1)k_{wx}}{2}L\right)Sa^2\left(\frac{q_y+(n\pm1)k_{wy}}{2}L\right)Sa^2\left(\frac{\omega+(n\pm1)\omega_w}{2}T\right) +Sa^2\left(\frac{q_x-(n\pm1)k_{wx}}{2}L\right)Sa^2\left(\frac{q_y-(n\pm1)k_{wy}}{2}L\right)Sa^2\left(\frac{\omega-(n\pm1)\omega_w}{2}T\right)\right\} \quad (23)$$

$$S_{32}(\omega) = -\frac{1}{2}Sa^2\left(\frac{q_x\pm nk_{wx}}{2}L\right)Sa^2\left(\frac{q_y\pm nk_{wy}}{2}L\right)Sa^2\left(\frac{\omega\pm n\omega_w}{2}T\right) \quad (24)$$

$$S_{33}(\omega) = \frac{1}{4}\left\{Sa^2\left(\frac{q_x+(n\pm2)k_{wx}}{2}L\right)Sa^2\left(\frac{q_y+(n\pm2)k_{wy}}{2}L\right)Sa^2\left(\frac{\omega+(n\pm2)\omega_w}{2}T\right) +Sa^2\left(\frac{q_x-(n\pm2)k_{wx}}{2}L\right)Sa^2\left(\frac{q_y-(n\pm2)k_{wy}}{2}L\right)Sa^2\left(\frac{\omega-(n\pm2)\omega_w}{2}T\right)\right\} \quad (25)$$

2.3. The NRCS of the Echo from a Sinusoidal Wave

If we integrate the spectra with respect to the angle frequency, the NRCS up to the third order is obtained as

$$\begin{aligned}\sigma &= \int_{-\infty}^{+\infty} S_1(\omega)\mathrm{d}\omega + \int_{-\infty}^{+\infty} S_2(\omega)\mathrm{d}\omega + \int_{-\infty}^{+\infty} S_3(\omega)\mathrm{d}\omega \\ &= \sigma_1 + \sigma_2 + \sigma_3 \end{aligned} \tag{26}$$

where σ_1, σ_2 and σ_3 denote the first-, second- and third-order NRCSs, respectively. And their expressions are

$$\begin{aligned}\sigma_1 &= 4\pi R^2 |Ka_0|^2 \exp\left(-\frac{q_z^2 a^2}{2}\right) \sum_{n=0}^{\infty}\sum_{r=0}^{\infty} \frac{\left(q_z^2 a^2\right)^{2r+n}}{2^{4r+2n}} \frac{1}{r!(r+n)!} \\ &\quad \cdot \left\{ Sa^2\left(\frac{q_x \pm nk_{wx}}{2}L\right) Sa^2\left(\frac{q_y \pm nk_{wy}}{2}L\right)\right\}, \end{aligned} \tag{27}$$

$$\begin{aligned}\sigma_2 &= 2\pi R^2 |K|^2 a^2 q_z \exp\left(-\frac{q_z^2 a^2}{2}\right) \left\{\mathrm{Re}\left(a_0 a_1^*\right) k_{wx} + \mathrm{Re}\left(a_0 a_2^*\right) k_{wy}\right\} \sum_{n=0}^{\infty}\sum_{r=0}^{\infty} \frac{\left(q_z^2 a^2\right)^{2r+n}}{2^{4r+2n}} \frac{1}{r!(r+n)!} \\ &\quad \cdot \left\{ Sa^2\left(\frac{q_x + (n\pm 1)k_{wx}}{2}L\right) Sa^2\left(\frac{q_y + (n\pm 1)k_{wy}}{2}L\right)\right. \\ &\quad \left. -Sa^2\left(\frac{q_x - (n\pm 1)k_{wx}}{2}L\right) Sa^2\left(\frac{q_y - (n\pm 1)k_{wy}}{2}L\right)\right\} \end{aligned} \tag{28}$$

and

$$\begin{aligned}\sigma_3 &= \pi R^2 |K|^2 a^4 q_z^2 \left(k_{wx}^2 a_1 a_1^* + 2k_{wx}k_{wy}\mathrm{Re}\left(a_1 a_2^*\right) + k_{wy}^2 a_2 a_2^*\right) \exp\left(-\frac{q_z^2 a^2}{2}\right) \\ &\quad \cdot \sum_{n=0}^{\infty}\sum_{r=0}^{\infty} \frac{\left(q_z^2 a^2\right)^{2r+n}}{2^{4r+2n}} \frac{1}{r!\,(r+n)!} \left\{\sigma_{31} + \sigma_{32} + \sigma_{33}\right\} \end{aligned} \tag{29}$$

with

$$\begin{aligned}\sigma_{31} &= Sa^2\left(\frac{q_x + (n\pm 1)\,k_{wx}}{2}L\right) Sa^2\left(\frac{q_y + (n\pm 1)\,k_{wy}}{2}L\right) \\ &\quad + Sa^2\left(\frac{q_x - (n\pm 1)\,k_{wx}}{2}L\right) Sa^2\left(\frac{q_y - (n\pm 1)\,k_{wy}}{2}L\right) \end{aligned} \tag{30}$$

$$\sigma_{32} = -\frac{1}{2} Sa^2\left(\frac{q_x \pm nk_{wx}}{2}L\right) Sa^2\left(\frac{q_y \pm nk_{wy}}{2}L\right) \tag{31}$$

$$\begin{aligned}\sigma_{33} &= \frac{1}{4} Sa^2\left(\frac{q_x + (n\pm 2)\,k_{wx}}{2}L\right) Sa^2\left(\frac{q_y + (n\pm 2)\,k_{wy}}{2}L\right) \\ &\quad + Sa^2\left(\frac{q_x - (n\pm 2)\,k_{wx}}{2}L\right) Sa^2\left(\frac{q_y - (n\pm 2)\,k_{wy}}{2}L\right) \end{aligned} \tag{32}$$

3. THE NUMERICAL RESULTS AND DISCUSSIONS

The wave tank experiments were carried out by Wen and Li in [27] to study the characteristics of electromagnetic backscattering from a sinusoidal water wave. The radar wave length λ_e is 0.88 m. The transmitting and receiving antennas are both V polarized, and the grazing angle is about 3 degrees. The other parameters of the water waves are shown in Table 1. Here, $\lambda_B = \lambda_e/(2\sin\theta_i) \approx \lambda_e/2$ denotes the first-order Bragg resonant wavelength. f_B is the Doppler shift of the first-order Bragg resonant scattering field. The Doppler spectra of the backscattering fields from sinusoidal water waves

for different wavelengths are shown in Fig. 1. From Fig. 1, one can find that not only the spectral peaks correspond to Bragg scattering (i.e., the peaks at $f_D = f_B$, $f_D = 1.41f_B$, $f_D = 1.73f_B$ and $f_D = 2f_B$ in Figs. 1(a)–(d), respectively) but other harmonic peaks can be found.

Table 1. Parameters of the water wave and calculated Doppler shift.

Water wave length L_1	λ_B	$2\lambda_B$	$3\lambda_B$	$4\lambda_B$
The normalized Doppler shift f_D/f_B of the Bragg scattering field	1.00	1.41	1.73	2.00

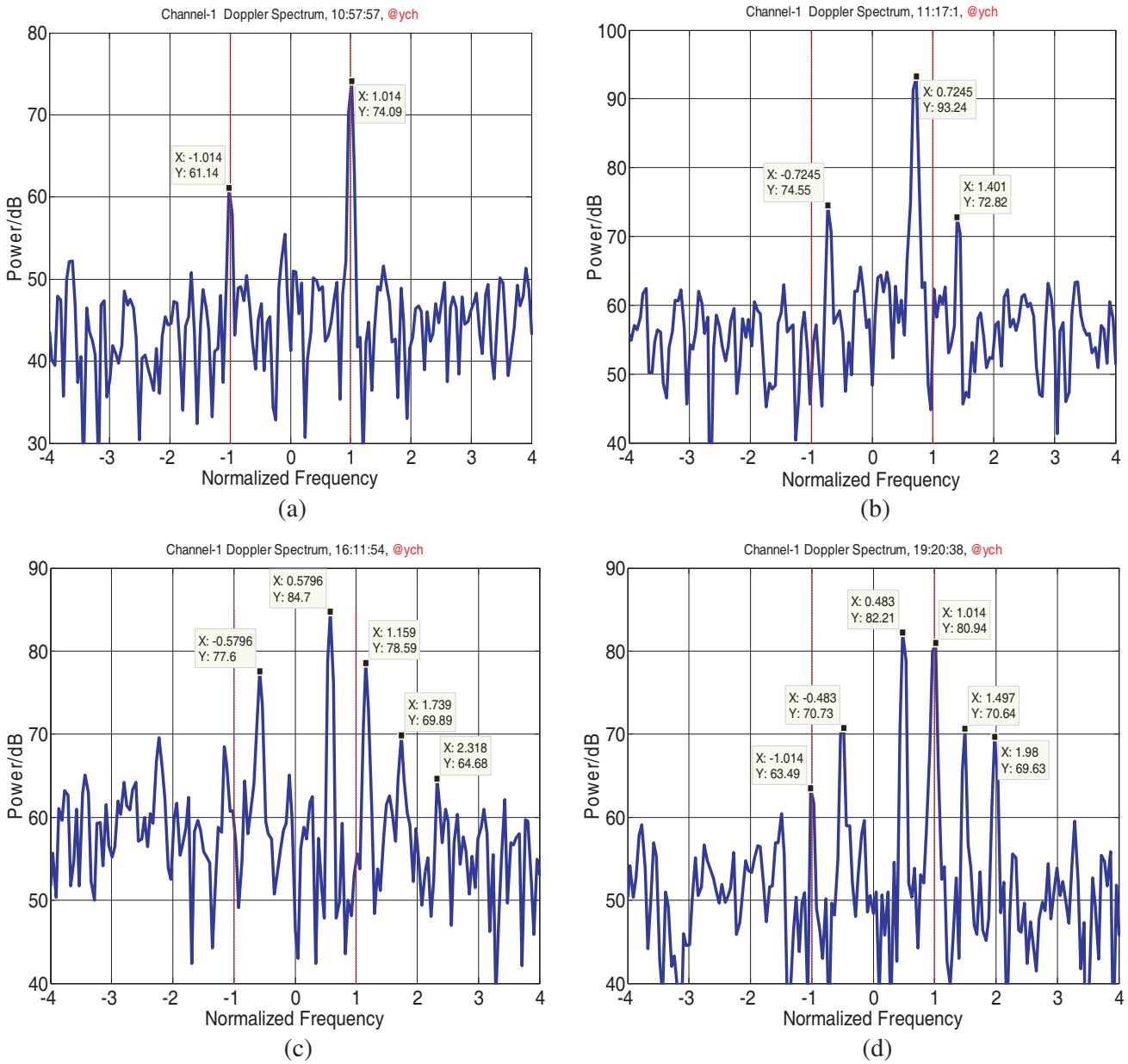

Figure 1. Doppler spectra of the backscattering fields from the sinusoidal water waves for different wavelengths measured by Wen et al. in [27]. (a) f_B, (b) $2f_B$, (c) $3f_B$, (d) $4f_B$.

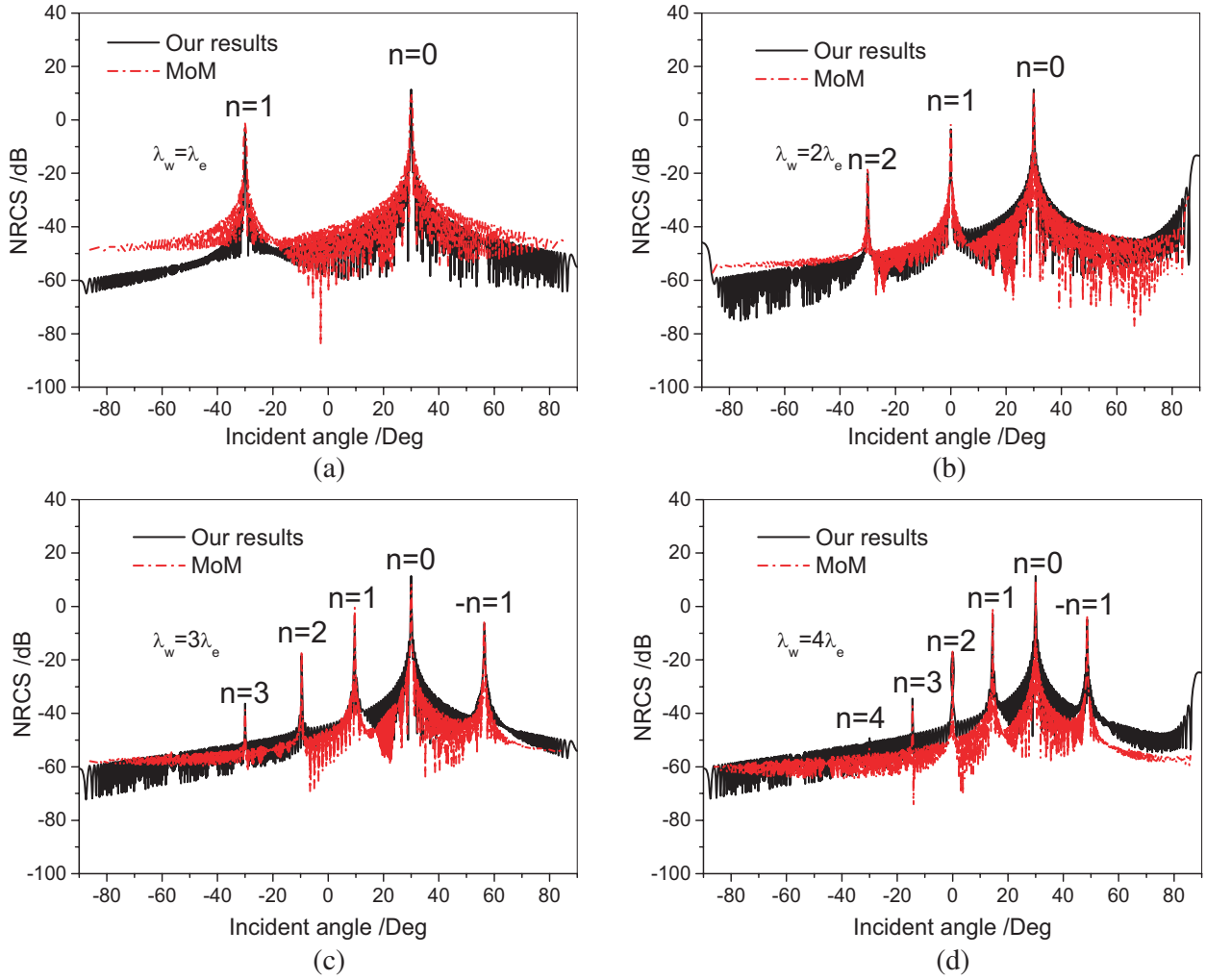

Figure 2. The bistatic HH-polarized NRCS from sinusoidal waves with different wavelengths.

In order to further reveal the properties of the scattering from sinusoidal water waves, the NRCS and Doppler spectra simulated by the higher-order Kirchhoff approximation are presented as follows. MoM is considered as an exact numerical method to calculate electromagnetic scattering from target [28]. Thus, the bistatic NRCS simulated by Eq. (26) is firstly compared with the numerical results by MoM in Fig. 2 to verify the validity of the theoretical model. In simulations, sinusoidal waves propagate along x axis, and the wave amplitude is set to $0.05\lambda_e$. The wavelength of electromagnetic wave $\lambda_e = 1\,\mathrm{m}$ and incident angle $\theta_i = 30°$. As shown in Fig. 2, if the scattering angle satisfies the relationship $\sin\theta_s = \sin\theta_i \pm nk_{wx}/k_e$, the Bragg resonant peaks would be found at this scattering angle. With the increase of water wavelength, more and more higher-order resonant peaks appear. On the other hand, the intensity of the resonant peaks decreases with the absolute value of order number n.

The influences of higher-order scattering fields induced by the local slope on the bistatic and monostatic NRCS are shown in Fig. 3 and Fig. 4, respectively. Here, the sinusoidal waves propagate along x axis, and the wave amplitude is set to $0.05\lambda_e$. For bistatic cases, the radar incident angle is 30°. From Fig. 3, we can find that the influence of the third-order field on the bistatic NRCS is not significant. When the water wavelength is longer, just as expected, the bistatic and monostatic NRCSs are both dominated by the first-order field. However, if the water wavelength is shorter, the surface slope is larger, and the second-order field would have an obviously impact on the Bragg resonant peak at $\theta_s = -30°$ in Fig. 3(a). For monostatic cases, if the water wavelength is shorter, the third-order field would make a significant impact on the NRCS at larger scattering angles from 70° to 90°. Meanwhile,

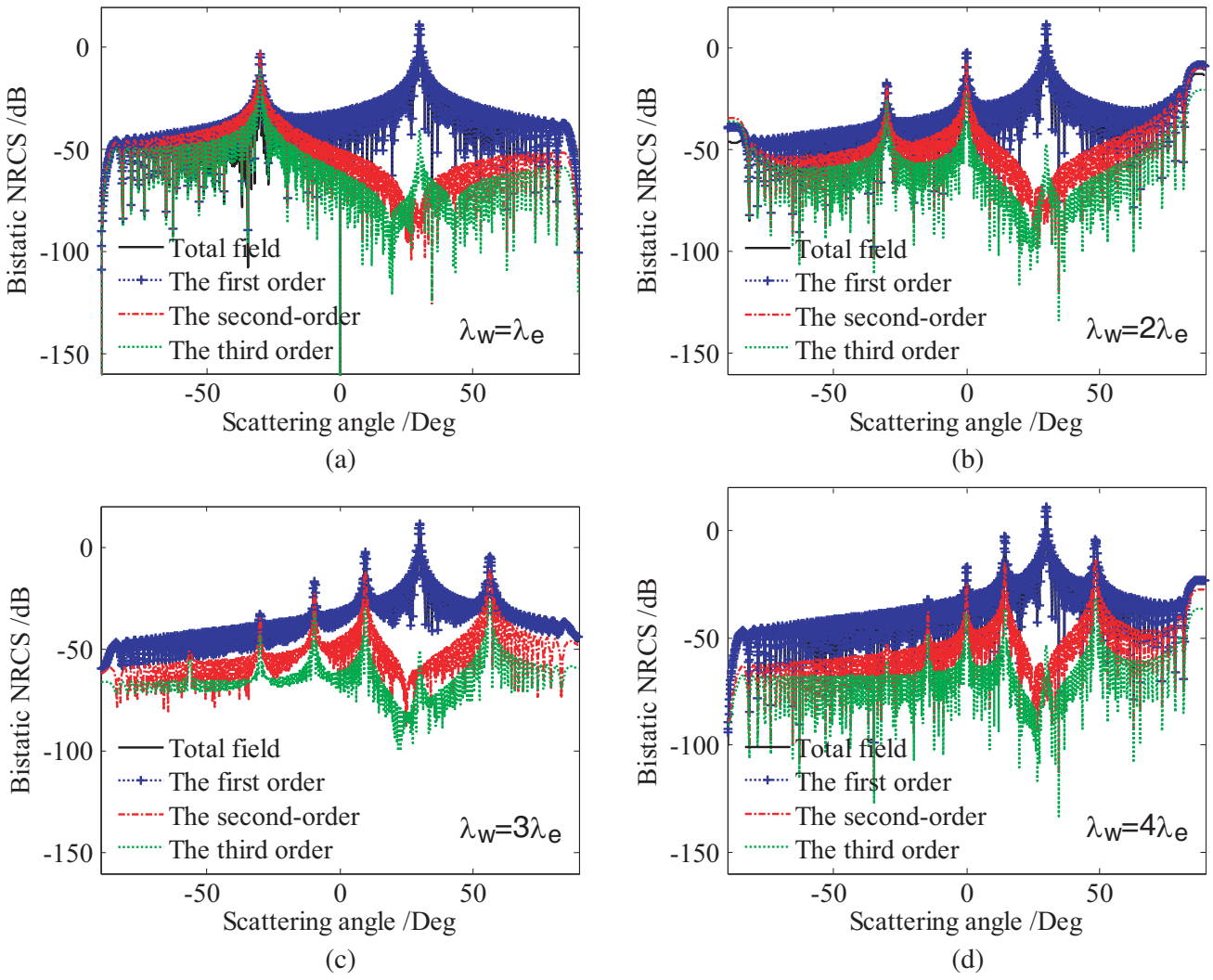

Figure 3. The influence of the higher-order scattering fields on the total power (Bistatic cases).

as shown in Figs. 4(a) and (b), the Bragg resonant peaks are also significantly affected by the higher-order fields. However, if the wavelength is longer, as shown in Figs. 3(c)–(d) and Figs. 4(c)–(d), the slope-dependent higher-order fields can be neglected.

The influence of the water wave's amplitude on the resonant peak is shown in Fig. 5. Here, the wavelength of the sinusoidal waves is $4\lambda_e$. The curves in Fig. 5 show that more than one resonant peak appears, and the intensities of the peaks are proportional to the amplitude of the water wave. If the amplitude of the water wave is small, the higher order resonant peaks cannot be seen. These phenomena can be explained by Eq. (27). It is found that if the scattering angle satisfies the following relationship, i.e.,

$$2k_e \sin\theta_i = nk_{wx} \quad \text{with} \quad n = 0, 1, 2, \ldots, \tag{33}$$

a resonant peak will emerge at this angle from the sampling function in Eq. (27). Here, Eq. (33) can be simplified as $\sin\theta_i = n/8$ because the wavelength of the sinusoidal waves is $4\lambda_e$ and $k_{wx} = k_e/4$. Thus, in theory, eight resonant peaks corresponding to $n = 0, 1, 2, \ldots, 7$ are possibly found. However, from Fig. 5 we can find that the number of resonant peaks is less than eight because the values of the resonant peaks are also affected remarkably by the coefficient Γ_n in Eq. (27), i.e.,

$$\Gamma_n = 4\pi R^2 \left|Ka_0\right|^2 \exp\left(-2a^2k_z^2\right) \sum_{r=0}^{\infty} \frac{\left(a^2k_z^2\right)^{2r+|n|}}{r!(r+|n|)!} \tag{34}$$

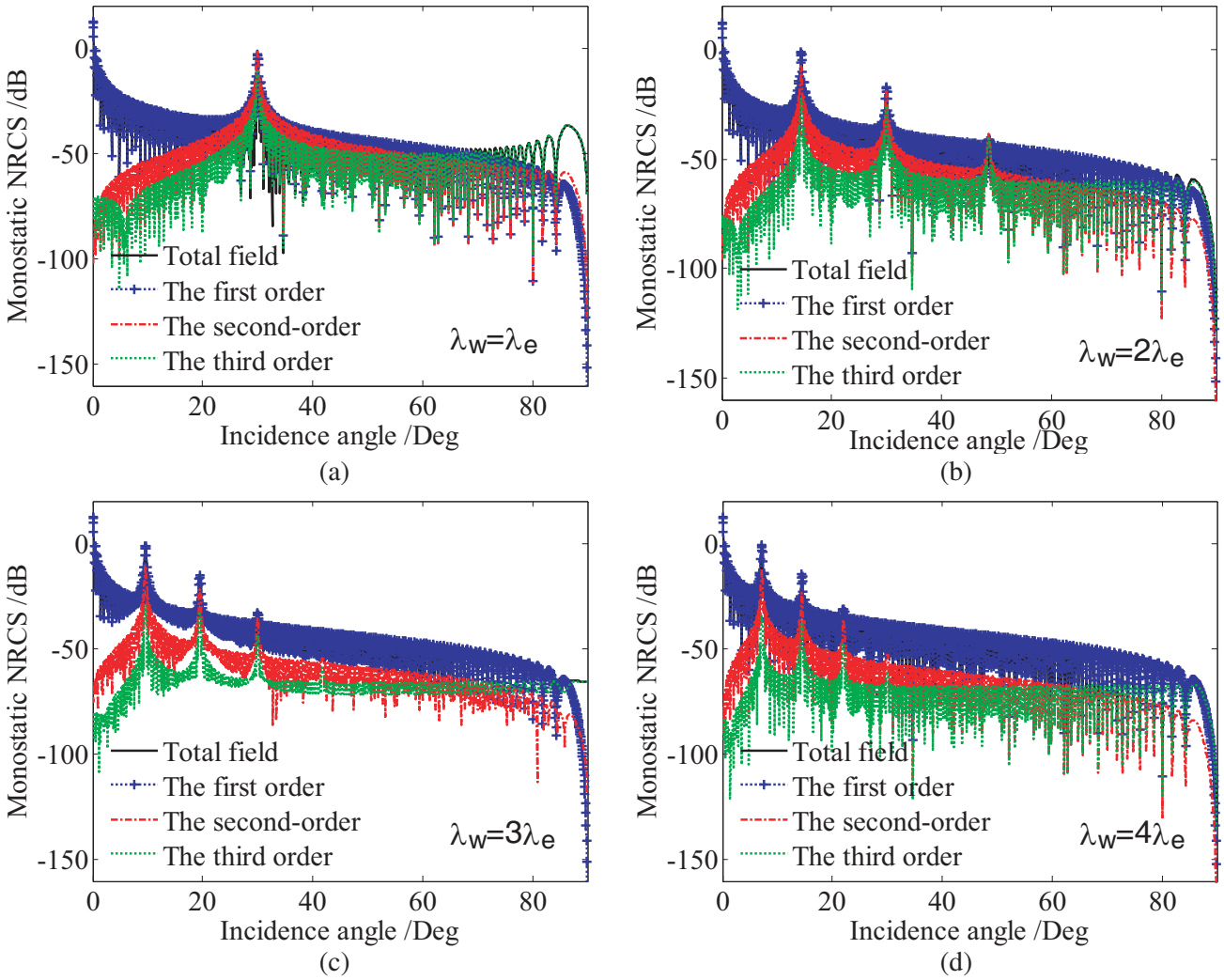

Figure 4. The influence of the higher-order scattering fields on the total power (Monostatic cases).

In order to show the influence of this coefficient, the values of Γ_n for different amplitudes of sinusoidal wave are shown in Fig. 6. The results in this figure demonstrate that if $n \neq 0$ the values of Γ_n increase with amplitude a and decrease with order number n. This property helps to explain why the values of the resonant peaks in Fig. 5 increase with the water wave amplitude a and decrease with incidence angle θ_i.

In Fig. 7, the Doppler spectra for the incoherent backscattering fields from sinusoidal wave with wavelength $\lambda_w = 3\lambda_e$ are presented. The amplitude of the water wave is set to $0.05\lambda_e$. In the left figure of Fig. 7, the resonant peaks and their orders are labeled by the order number n. From Fig. 7 we can find that not only the resonant peaks but also other equally spaced harmonic peaks can be found. However, comparing the harmonic peaks with the resonant peaks, it is shown that the values of the harmonic peaks are obviously smaller. In order to explain this phenomenon, we firstly rewrite the first-order expression of the Doppler spectrum as

$$S(f) = \sum_{n=-\infty}^{\infty} \Gamma_n \varsigma_n \xi_n \tag{35}$$

with

$$\varsigma_n = Sa^2 \left(\frac{q_x - nk_{wx}}{2} L \right) \tag{36}$$

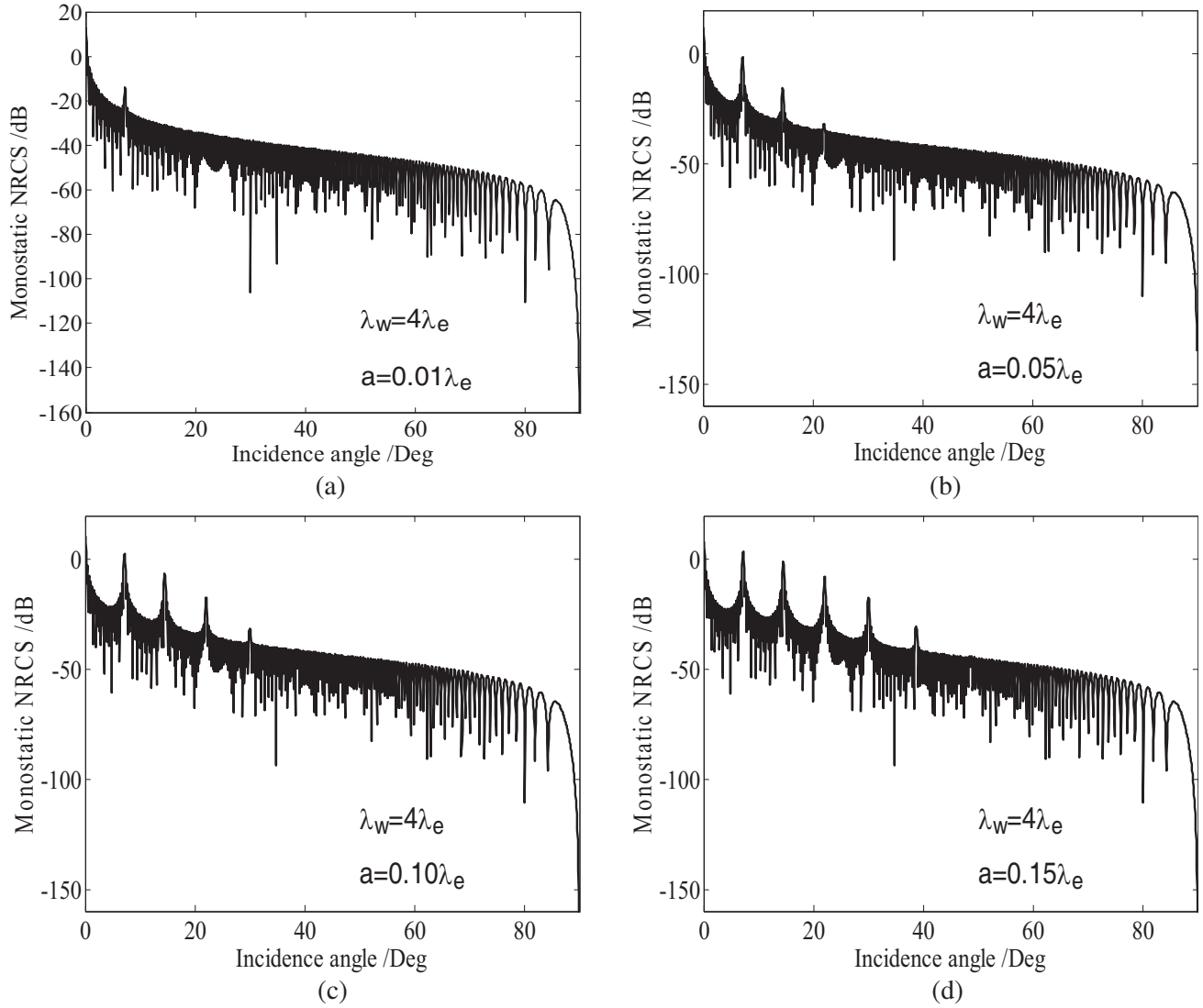

Figure 5. The resonant peaks of the monostatic scattering fields from sinusoidal waves with different amplitudes.

$$\xi_n = Sa^2[\pi(f - nf_w)T] \tag{37}$$

and the coefficient Γ_n is given by Eq. (34).

The phenomena of the Doppler spectrum shown in Fig. 7 can be well explained by Eq. (35). It is found that the Doppler spectra of the electromagnetic fields scattered from sinusoidal waves are determined by three terms, i.e., Γ_n, ς_n and ξ_n from Eq. (35). The influences of Γ_n are shown in Fig. 6. In order to illustrate the effect of the other two terms, their properties are presented in Fig. 8 and Fig. 9, respectively. Eq. (37) shows that positions of the peaks are decided by ξ_n in frequency domain. If the frequency f satisfies the following equation

$$f - nf_w = 0 \quad \text{for} \quad n = 0, \pm 1, \pm 2, \ldots \tag{38}$$

just as shown in Fig. 8, a peak would appear. However, we can also find that the peaks of ξ_n for different f are all equal to the same value. This means that the function ξ_n does not determine the values of the spectral peaks.

Compared with Γ_n and ξ_n, ς_n is another term which affects the values of the spectral peaks. And the position of the Bragg resonant peak is also determined by this term. Without loss of generality, the

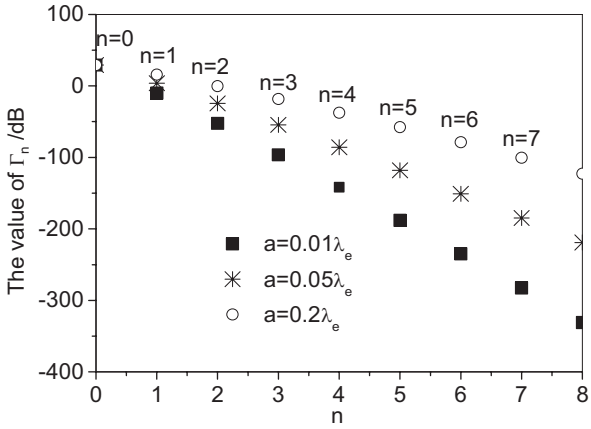

Figure 6. The values of Γ_n for different amplitudes of the water wave.

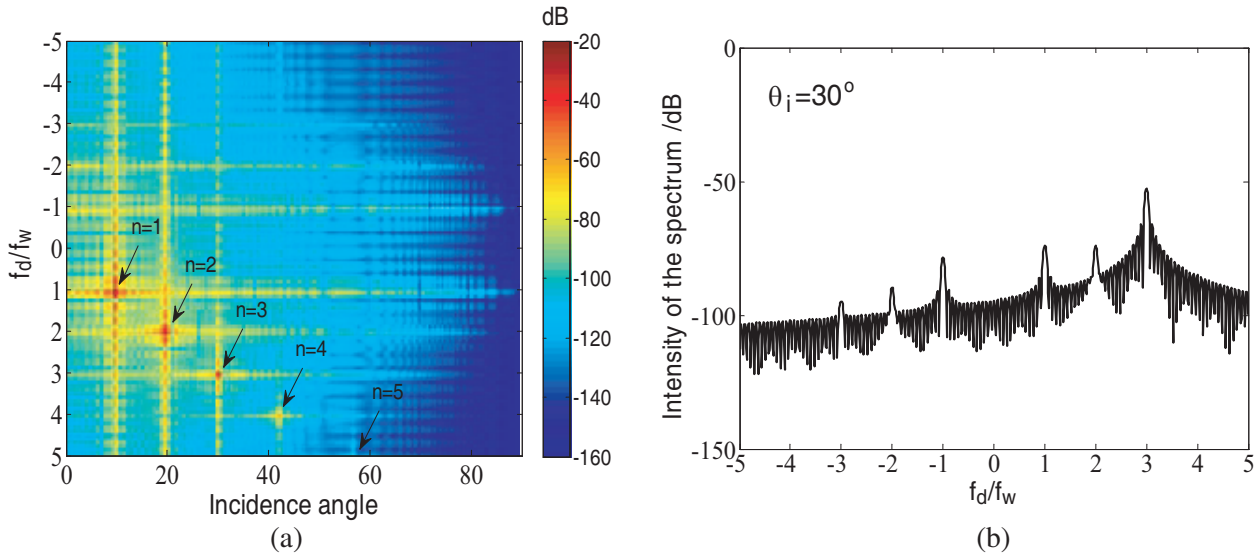

Figure 7. (a) The false-color image of the Doppler spectra from sinusoidal wave and (b) the spectra along the cross section $\theta_i = 30°$.

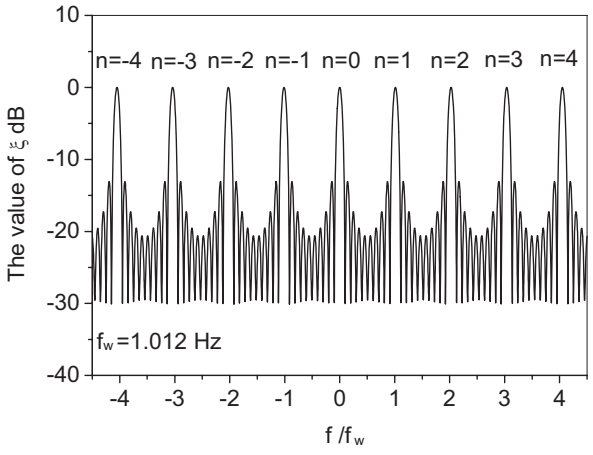

Figure 8. The value of ξ_n versus the normalized frequency f/f_w.

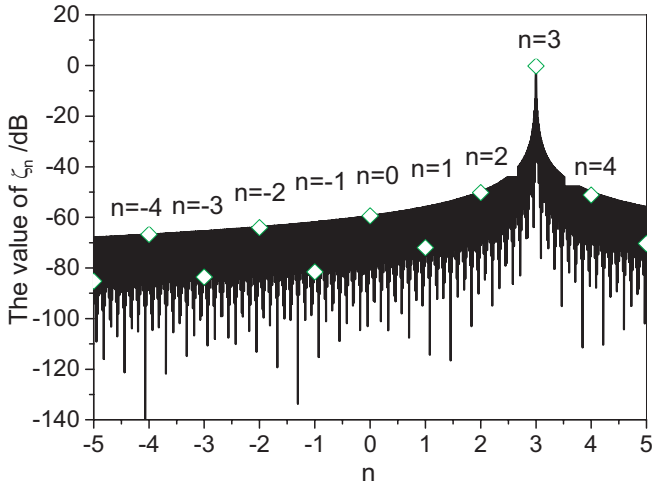

Figure 9. The value of ς_n as a function of n. The green diamonds on the black line denote the positions of the spectral peaks and the corresponding values of ς_n.

spatial wavenumber k_{wx} of the water wave is set to $k_e/3$. From Eq. (36) we can find that the sampling function ς_n has a peak if parameter n satisfies the equation $q_x - nk_{wx} = 0$. For example, a resonant peak would present at position $f = 3f_w$ when the incidence angle $\theta_i = 30°$ and integer $n = q_x/k_{wx} = 3$. However, if $n \neq 3$, by contrast, the values of ς_n are obviously smaller (see the green diamonds in Fig. 9). The properties of ς_n mentioned above mean that the position and value of the spectral peak are both affected by ς_n. Using these properties of ξ_n and ς_n above, the characteristics shown in Fig. 7 can be well explained.

4. CONCLUSIONS

In this paper, the scattering field from sinusoidal wave has been investigated by higher order KA. Firstly, the theoretical models for the NRCS and the Doppler spectrum are proposed, and the comparisons with the MoM results demonstrate that our theoretical models are reasonable, and the contributions of the slope-dependent higher order terms can be generally neglected if the slope of the sinusoidal wave is small. Secondly, it can be found that several resonant peaks would appear with the incidence angle from the curves of backscattering fields. The values of the resonant peaks increase with the amplitude of the sinusoidal wave and decrease with the incidence angle. On the other hand, it is shown that not only the spectral peak corresponding to the Bragg scattering can be seen but also some equally spaced harmonic peaks can also be found from the figure of the Doppler spectrum. The phenomena mentioned above can be successfully explained by the models proposed in the present work.

ACKNOWLEDGMENT

This work was supported in part by the National Natural Science Foundation of China under Grant 41576170 and 41376179, by the National Natural Science Foundation of China-Shandong Joint Fund for Marine Science Research Centers under Grant. U1606405.

REFERENCES

1. Holliday, D., "Resolution of a controversy surrounding the Kirchhoff approach and the small perturbation method in rough surface scattering theory," *IEEE Trans. Antennas Propag.*, Vol. 35, No. 1, 120–122, 1987.

2. Ishimaru, A. and J. S. Chen, "Scattering from very rough metallic and dielectric surfaces: a theory based on the modified Kirchhoff approximation," *Waves in Random Media*, Vol. 1, No. 1, 21–34, 1991.
3. Thorsos, E. I., "The validity of the perturbation approximation for rough surface scattering using a Gaussian roughness spectrum," *J. Acoust. Soc. Am.*, Vol. 86, No. 1, 261–277, 1989.
4. Soto-Crespo, J. M., M. Nieto-Vesperinas, and A. T. Friberg, "Scattering from slightly rough random surfaces: A detailed study on the validity of the small perturbation method," *J. Opt. Soc. Am. A*, Vol. 7, No. 7, 1185–1201, 1990.
5. Mouche, A. A., F. Collard, B. Chapron, K. F. Dagestad, G. Guitton, J. A. Johannessen, V. Kerbaol, and M. W. Hansen, "On the use of Doppler shift for sea surface wind retrieval from SAR," *IEEE Trans. Geosci. Remote Sensing*, Vol. 50, No. 7, 2901–2909, 2012.
6. Barrick, D. E., "Extraction of wave parameters from measured HF radar sea-echo Doppler spectra," *Radio Sci.*, Vol. 12, 415–424, 1977.
7. Johnson, J. T., R. J. Burkholder, J. V. Toporkov, D. R. Lyzenga, and W. J. Plant, "A numerical study of the retrieval of sea surface height profiles from low grazing angle radar data," *IEEE Trans. Geosci. Remote Sensing*, Vol. 47, No. 3, 1641–1650, 2009.
8. Hwang, P. A., M. A. Sletten, and J. V. Toporkov, "A note on Doppler processing of coherent radar backscatter from the water surface: With application to ocean surface wave measurements," *J. Geophys. Res.*, Vol. 115, C03026, 2010.
9. Chae, C. S. and J. T. Johnson, "A study of sea surface range-resolved Doppler spectra using numerically simulated low-grazing-angle backscatter data," *IEEE Trans. Geosci. Remote Sens.*, Vol. 51, No. 6, 3452–3460, 2013.
10. Wang, Y. H. and Y. M. Zhang, "The measurement of sea surface profile with X-band coherent marine radar," *Acta Oceanol. Sin.*, Vol. 34, No. 9, 65–70, 2015.
11. Chapron, B., F. Collard, and F. Ardhum, "Direct measurements of ocean surface velocity from space: Interpretation and validation," *J. Geophys. Res.*, Vol. 110, C07008, 2005.
12. Johannessen, J. A., V. Kudryavtsev, D. Akimov, T. Eldevik, N. Winther, and B. Chapron, "On radar imaging of current features; Part 2: Mesoscale eddy and current front detection," *J. Geophys. Res.*, Vol. 110, C07017, 2005.
13. Kudryavtsev, V., D. Akimov, J. A. Johannessen, and B. Chapron, "On radar imaging of current features. Part 1: Model and comparison with observations," *J. Geophys. Res.*, Vol. 110, C07016, 2005.
14. Karaev, V., M. Kanevsky, and E, Meshkov, "The effect of sea surface slicks on the Doppler spectrum width of a backscattered microwave signal," *Sensors*, Vol. 8, 3780–3801, 2008.
15. Mei, C. C., *Michael Stiassnie Theory and Applications of Ocean Surface Waves: Part I — Linear Aspect*, 3rd Edition, World Scientific Publishing, 2017.
16. Toporkov, J. V. and G. S. Brown, "Numerical simulations of scattering from time-varying randomly rough surfaces," *IEEE Trans. Geosci. Remote Sensing*, Vol. 38, No. 4, 1616–1625, 2000.
17. Johnson, J. T., J. V. Toporkov, and G. S. Brown, "A numerical study of backscattering from time-evolving sea surfaces: Comparison of hydrodynamic models," *IEEE Trans. Geosci. Remote Sensing*, Vol. 39, No. 11, 2411–2420, 2001.
18. Hayslip, A. R., J. T. Johnson, and G. R. Baker, "Further numerical studies of backscattering from time-evolving nonlinear sea surfaces," *IEEE Trans. Geosci. Remote Sensing*, Vol. 41, No. 10, 2287–2293, 2003.
19. Saillard, M., P. Forget, G. Soriano, M. Joelson, P. Broche, and P. Currier, "Sea surface probing with L-band Doppler radar: Experiment and theory," *C. R. Physique*, Vol. 6, 675–682, 2005.
20. Zavorotny, V. U. and A. G. Voronovich, "Two-scale model and ocean radar Doppler spectra at moderate- and low-grazing angles," *IEEE Trans. Antennas Propagat.*, Vol. 46, No. 1, 84–92, 1998.
21. Romeiser, R. and D. R. Thompson, "Numerical study on the Along-Track interferometric radar imaging mechanism of oceanic surface currents," *IEEE Trans. Geosci. Remote Senging*, Vol. 38, No. 1, 446–458, 2000.

22. Wang, Y. H., Y. M. Zhang, and C. F. Zhao, "Doppler spectra of microwave scattering fields from nonlinear oceanic surface at moderate- and low-grazing angles," *IEEE Trans. Geosci. Remote Sensing*, Vol. 50, No. 4, 1104–1116, 2012.
23. Wang, Y. H., Y. M. Zhang, and L. X. Guo, "Microwave Doppler spectra of sea echoes at high incidence angles: Influences of large-scale waves," *Progress In Electromagnetics Research B*, Vol. 48, 99–113, 2013.
24. Wang, Y. H., Y. M. Zhang, H. M. Li, and G. Chen, "Doppler spectrum of microwave SAR signals from two-dimensional time-varying sea surface," *Journal of Electromagnetic Waves and Applications*, Vol. 30, No. 10, 1265–1276, 2016.
25. Miret, D., G. Soriano, F. Nouguier, et al., "Sea surface microwave scattering at extreme grazing angle: Numerical investigation of the Doppler shift," *IEEE Trans. Geosci. Remote Sensing*, Vol. 52, No. 11, 7120–7129, 2014.
26. Ulaby, F. T., R. K. Moore, and A. K. Fung, *Microwave Remote Sensing: Volume II Radar Remote Sensing and Surface Scattering and Emission Theory*, Artech House, 1986.
27. Wen, B. Y. and K. Li, "Frequency shift of the Bragg and non-Bragg backscattering from periodic water wave," *Scientific Reports*, 1–7, 2016.
28. Franceschetti, G., A. Iodice, and D. Riccio, "Scattering from dielectric random fractal surfaces via Method of Moments," *IEEE Trans. Antennas Propag.*, Vol. 38, No. 4, 1644–1655, 2000.